Article – SUPPLEMENTARY MATERIAL

An evaluation of the CHIMERE chemistry transport model to simulate dust outbreaks across the north Hemisphere in March 2014

Bertrand Bessagnet [1*], Laurent Menut [2], Augustin Colette [1], Florian Couvidat [1], Mo Dan [3], Sylvain Mailler [2,4], Laurent Létinois [1], Véronique Pont [5], Laurence Rouïl [1]

[1] INERIS, National Institute for Industrial Environment and Risks, Parc Technologique ALATA, 60550 Verneuil-en-Halatte, France
[2] Laboratoire de Météorologie Dynamique, Ecole Polytechnique, PSL Research University, Ecole Normale Supérieure, Université Paris-Saclay, Sorbonne Universités, UPMC University Paris 06, CNRS, Route de Saclay, 91128 Palaiseau, France
[3] Central Laboratory, Beijing Municipal Institute of Labour Protection, Room 317, 55 Taoranting Road, Xicheng District, Beijing 100054, China
[4] École des Ponts ParisTech, Université Paris-Est, 77455 Champs-sur-Marne, France
[5] Laboratoire d'Aérologie, 14 Avenue Edouard Belin, 31400 Toulouse, Université de Toulouse, CNRS, UPS, France
* Correspondence: bertrand.bessagnet@ineris.fr; Tel.: +33-3-44-55-65-33

LIST OF TABLES AND FIGURES

Tables

Figures

Table S1. Error statistics (Correlation, Root Mean Square Error - RMSE, Bias) for CHIMERE at several AERONET stations over the north Hemisphere for March 2014

Site	N*	Obs.	Mod.	Cor.	RMSE^{+}	Bias
Boulder	115	0.03	0.12	0.02	6.91	0.09
Yuma	221	0.06	0.11	0.10	2.40	0.06
Red Mountain	127	0.01	0.06	0.12	38.48	0.05
Barbados	120	0.10	0.15	0.33	2.03	0.05
UPRM	160	0.07	0.10	0.27	1.48	0.02
Cape San Juan	255	0.07	0.13	0.09	1.89	0.06
Petrolina	114	0.06	0.03	0.20	0.50	-0.03
Calhau	102	0.09	0.14	0.70	2.92	0.05
Capo Verde	98	0.13	0.22	0.79	2.64	0.09
Edinburgh	65	0.04	0.32	-0.20	9.58	0.27
Graciosa	69	0.07	0.22	0.04	3.06	0.15
Coruna	40	0.05	0.14	0.42	2.29	0.09
Toulouse	137	0.06	0.50	0.04	14.15	0.45
Cabauw	113	0.15	0.71	0.07	8.82	0.56
Dushanbe	53	0.09	0.46	0.29	5.49	0.37
Jaipur	203	0.24	0.29	-0.27	1.26	0.06
Qoms	224	0.02	0.35	0.09	25.16	0.33
Dalanzadgad	197	0.08	0.65	0.24	16.23	0.57
XiangHe	162	0.40	0.68	0.11	5.57	0.28
Gosan	113	0.17	0.39	-0.11	5.11	0.22
Noto	63	0.15	0.41	0.09	2.88	0.25
Mauna	171	0.01	0.06	0.32	5.16	0.04
Midway	70	0.07	0.31	0.15	5.35	0.24
Izana	243	0.01	0.12	0.46	15.27	0.11
Dakar	258	0.26	0.20	0.76	0.35	-0.06
Camaguey	152	0.08	0.13	0.62	0.88	0.04
Beijing	179	0.47	0.63	-0.07	3.98	0.17
Ieodo	87	0.15	0.36	0.41	2.36	0.21
Pokhara	140	0.20	0.38	0.00	1.64	0.18
Cinzana	287	0.32	0.21	0.60	0.51	-0.11
Murcia	213	0.09	0.21	0.85	5.78	0.12
Average		*Cor_s^{**}=0.54*		*0.24*	*6.46*	*0.16*

**Number of available hourly observations, $^{+}$Root mean Square Error, **Spatial correlation*

Table S2. Characteristics, locations of EBAS-EMEP sites used in this study

Site code	Site name	Lon E (°)	Lat N (°)	Alt. (m)
AM01	AM0001R	44.26	40.38	2080
AT02	AT0002R	16.77	47.77	117
AT05	AT0005R	12.97	46.68	1020
AT48	AT0048R	14.44	47.84	899
CH01	CH0001G	7.99	46.55	3578
CH02	CH0002R	6.94	46.81	489
CH03	CH0003R	8.90	47.48	539
CH04	CH0004R	6.98	47.05	1137
CH05	CH0005R	8.46	47.07	1031
CY02	CY0002R	33.06	35.04	532
CZ03	CZ0003R	15.08	49.57	535
CZ05	CZ0005R	13.60	49.07	1118
DE43	DE0043G	11.01	47.80	985
DE44	DE0044R	12.93	51.53	86
DK03	DK0003R	9.60	56.35	13
DK12	DK0012R	12.09	55.69	3
EE09	EE0009R	25.90	59.50	32
EE11	EE0011R	21.82	58.38	6
ES01	ES0001R	-4.35	39.55	917
ES05	ES0005R	-8.92	42.73	683
ES07	ES0007R	-3.53	37.23	1265
ES08	ES0008R	-4.85	43.44	134
ES09	ES0009R	-3.14	41.28	1360
ES10	ES0010R	3.32	42.32	23
ES11	ES0011R	-6.92	38.48	393
ES12	ES0012R	-1.10	39.09	885
ES13	ES0013R	-5.87	41.28	985
ES14	ES0014R	0.72	41.40	470
ES16	ES0016R	-7.70	43.23	506
ES17	ES0017R	-6.33	37.03	5
FI09	FI0009R	21.38	59.78	7
FI18	FI0018R	27.67	60.53	4
FI36	FI0036R	24.24	68.00	340
FR09	FR0009R	4.63	49.90	390
FR10	FR0010R	4.08	47.27	620
FR13	FR0013R	0.18	43.62	200
FR14	FR0014R	6.83	47.30	836
FR15	FR0015R	-0.75	46.65	133
FR18	FR0018R	-0.45	48.63	309
FR23	FR0023R	5.28	44.57	605
FR24	FR0024R	-1.84	47.83	29
FR25	FR0025R	2.61	46.81	182
GB06	GB0006R	-7.87	54.44	126
GB36	GB0036R	-1.32	51.57	137
GB43	GB0043R	-4.69	51.78	160
GB48	GB0048R	-3.24	55.79	260
HU02	HU0002R	19.58	46.97	125
IE01	IE0001R	-10.24	51.94	11
IE05	IE0005R	-6.92	52.87	59
IE06	IE0006R	-7.34	55.38	20
IE08	IE0008R	-6.36	52.18	9
IT01	IT0001R	12.63	42.10	48
LV10	LV0010R	21.17	56.16	18
MD13	MD0013R	28.28	46.49	166
MK07	MK0007R	20.69	41.54	1332
NL07	NL0007R	6.57	52.08	20
NL09	NL0009R	6.28	53.33	1
NL10	NL0010R	5.85	51.54	28
NL44	NL0644R	4.92	51.97	1
NL91	NL0091R	4.50	52.30	4
NO02	NO0002R	8.25	58.39	219
NO15	NO0015R	13.92	65.83	439
NO39	NO0039R	8.88	62.78	210
NO42	NO0042G	11.89	78.91	474
NO56	NO0056R	11.08	60.37	300
RO08	RO0008R	25.13	47.32	908
SE05	SE0005R	15.33	63.85	404
SE11	SE0011R	13.15	56.02	175
SE12	SE0012R	17.38	58.80	20
SE14	SE0014R	11.91	57.39	5
SI08	SI0008R	14.87	45.57	520
SK06	SK0006R	22.27	49.05	345

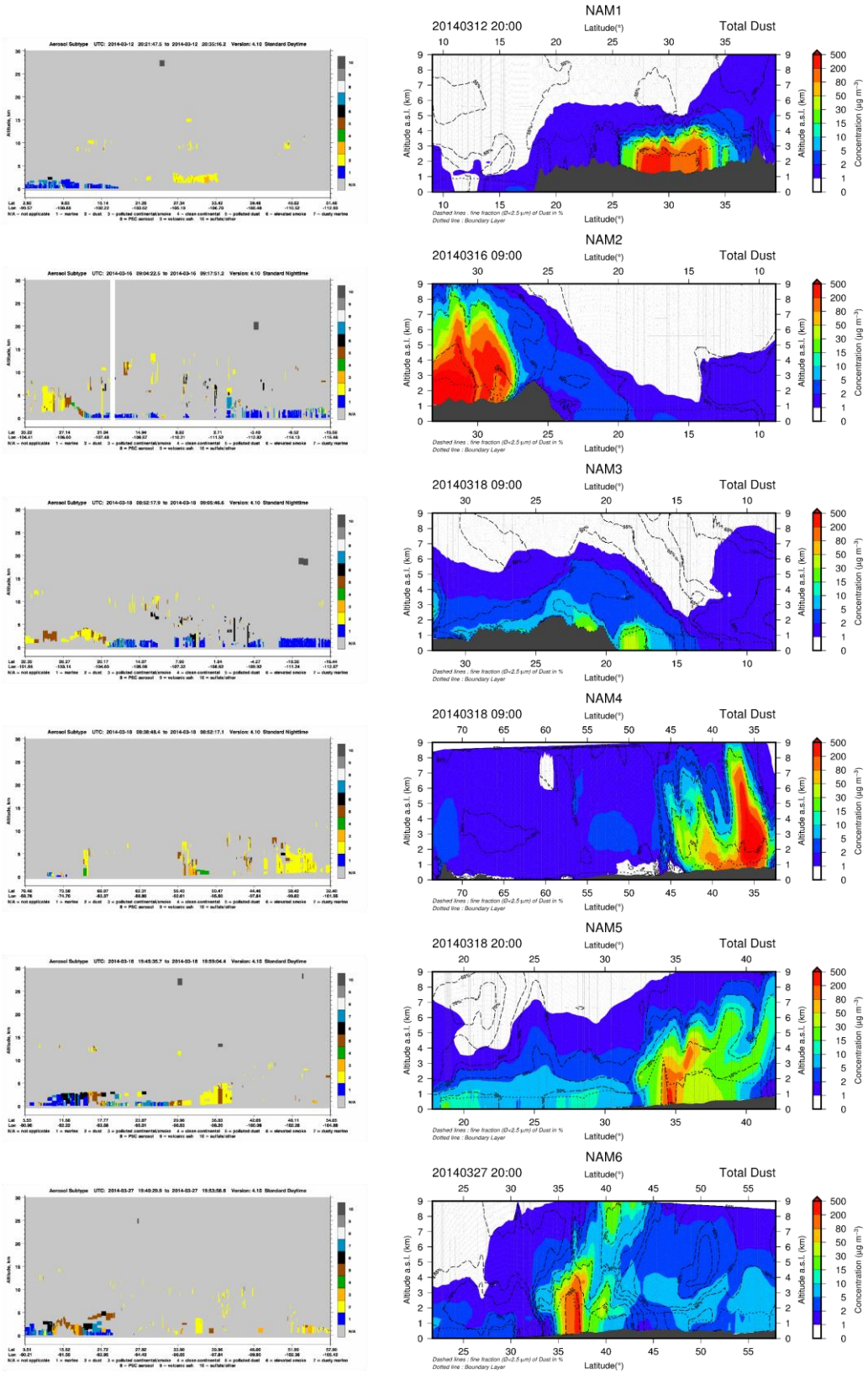

Figure S1. Cross sections of CHIMERE dust concentrations (right) for several orbits zoomed over the highest values area *versus* the corresponding CALIPSO qualitative data (left) showing in yellow the dust load and in orange the polluted dust, for the CALIPSO trajectories NAM1-6 as reported in Figure 2 in the publication. The dotted line represents the height of the boundary layer, the dashed lines represent the fraction of fine dust in %.

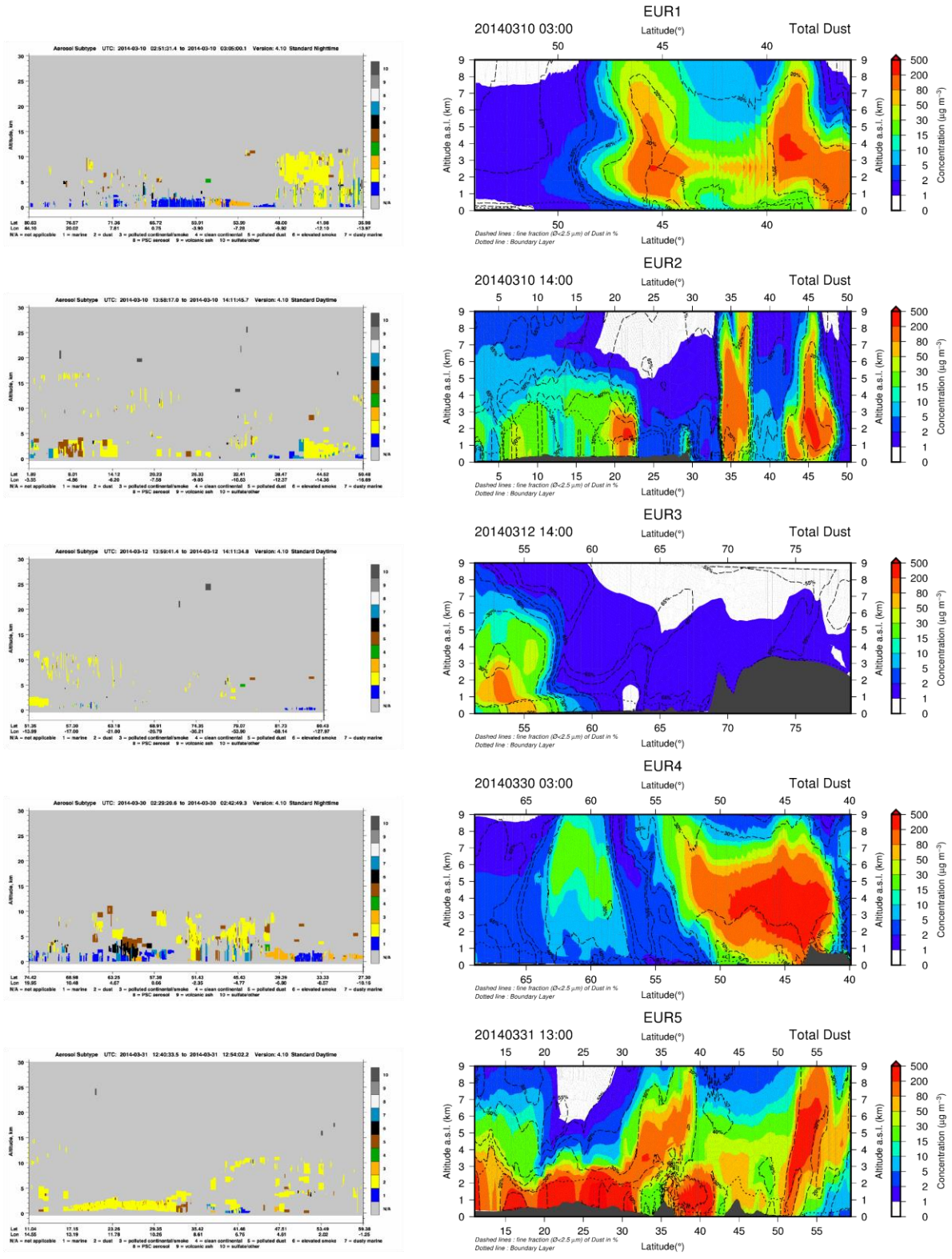

Figure S2. Cross sections of CHIMERE dust concentrations (right) for several orbits zoomed over the highest values area *versus* the corresponding CALIPSO qualitative data (left) showing in yellow the dust load and in orange the polluted dust, for the CALIPSO trajectories EUR1-5 as reported in Figure 2 in the publication. The dotted line represents the height of the boundary layer, the dashed lines represent the fraction of fine dust in %.

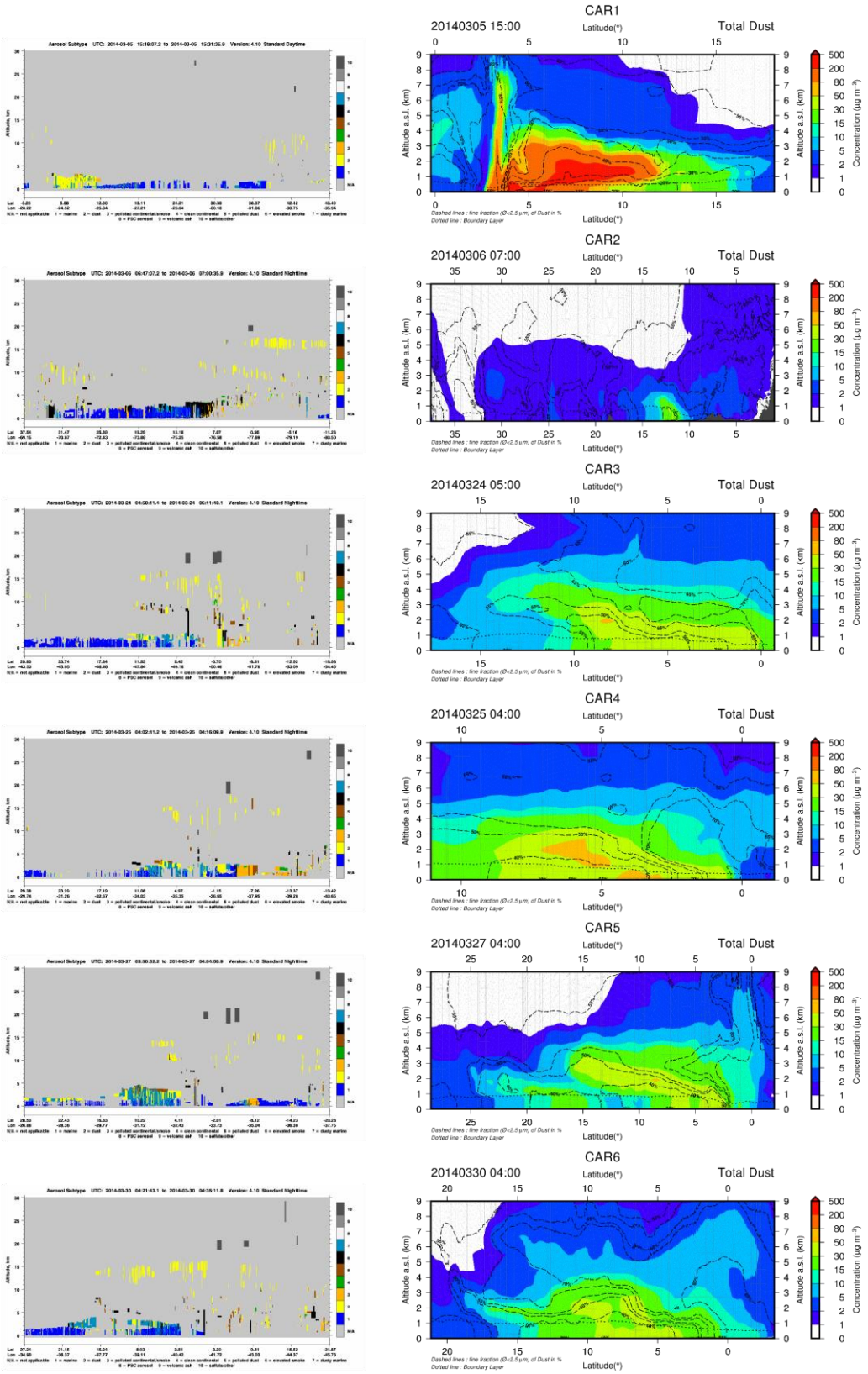

Figure S3. Cross sections of CHIMERE dust concentrations (right) for several orbits zoomed over the highest values area *versus* the corresponding CALIPSO qualitative data (left) showing in yellow the dust load and in orange the polluted dust, for the CALIPSO trajectories CAR1-6 as reported in Figure 2 in the publication. The dotted line represents the height of the boundary layer, the dashed lines represent the fraction of fine dust in %.

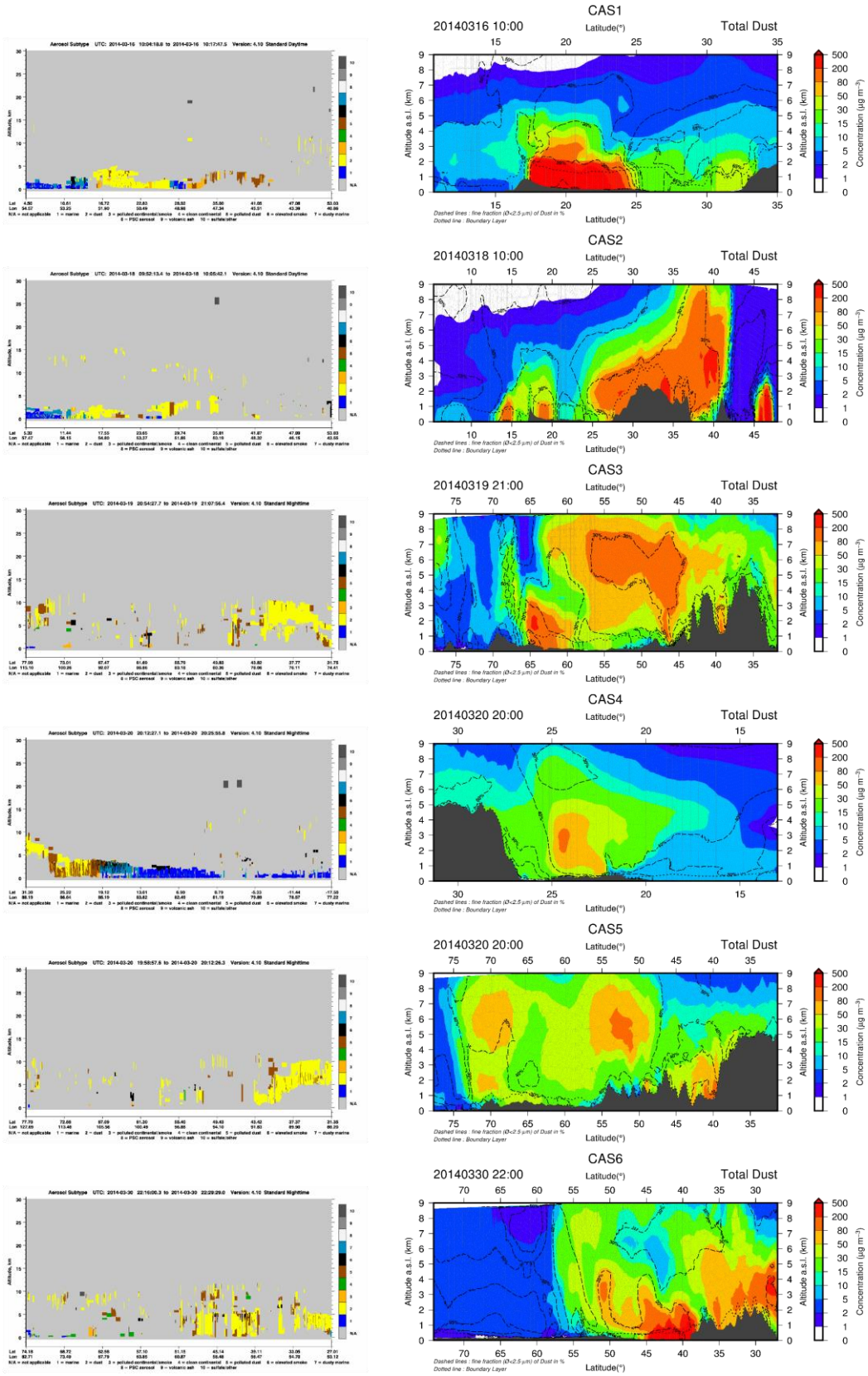

Figure S4. Cross sections of CHIMERE dust concentrations (right) for several orbits zoomed over the highest values area *versus* the corresponding CALIPSO qualitative data (left) showing in yellow the dust load and in orange the polluted dust, for the CALIPSO trajectories CAS1-6 as reported in Figure 2 in the publication. The dotted line represents the height of the boundary layer, the dashed lines represent the fraction of fine dust in %.

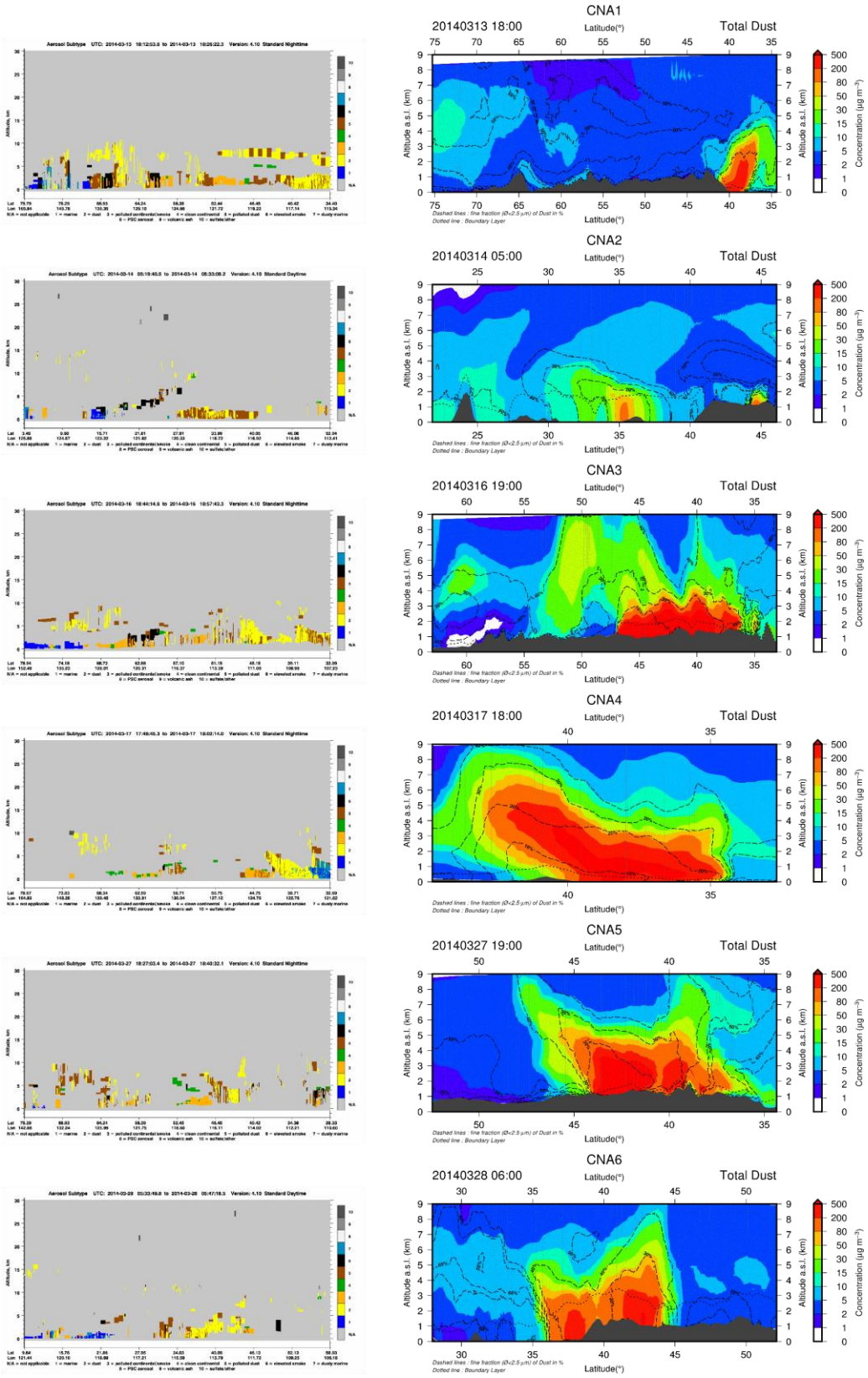

Figure S5. Cross sections of CHIMERE dust concentrations (right) for several orbits zoomed over the highest values area *versus* the corresponding CALIPSO qualitative data (left) showing in yellow the dust load and in orange the polluted dust, for the CALIPSO trajectories CNA1-6 as reported in Figure 2 in the publication. The dotted line represents the height of the boundary layer, the dashed lines represent the fraction of fine dust in %.

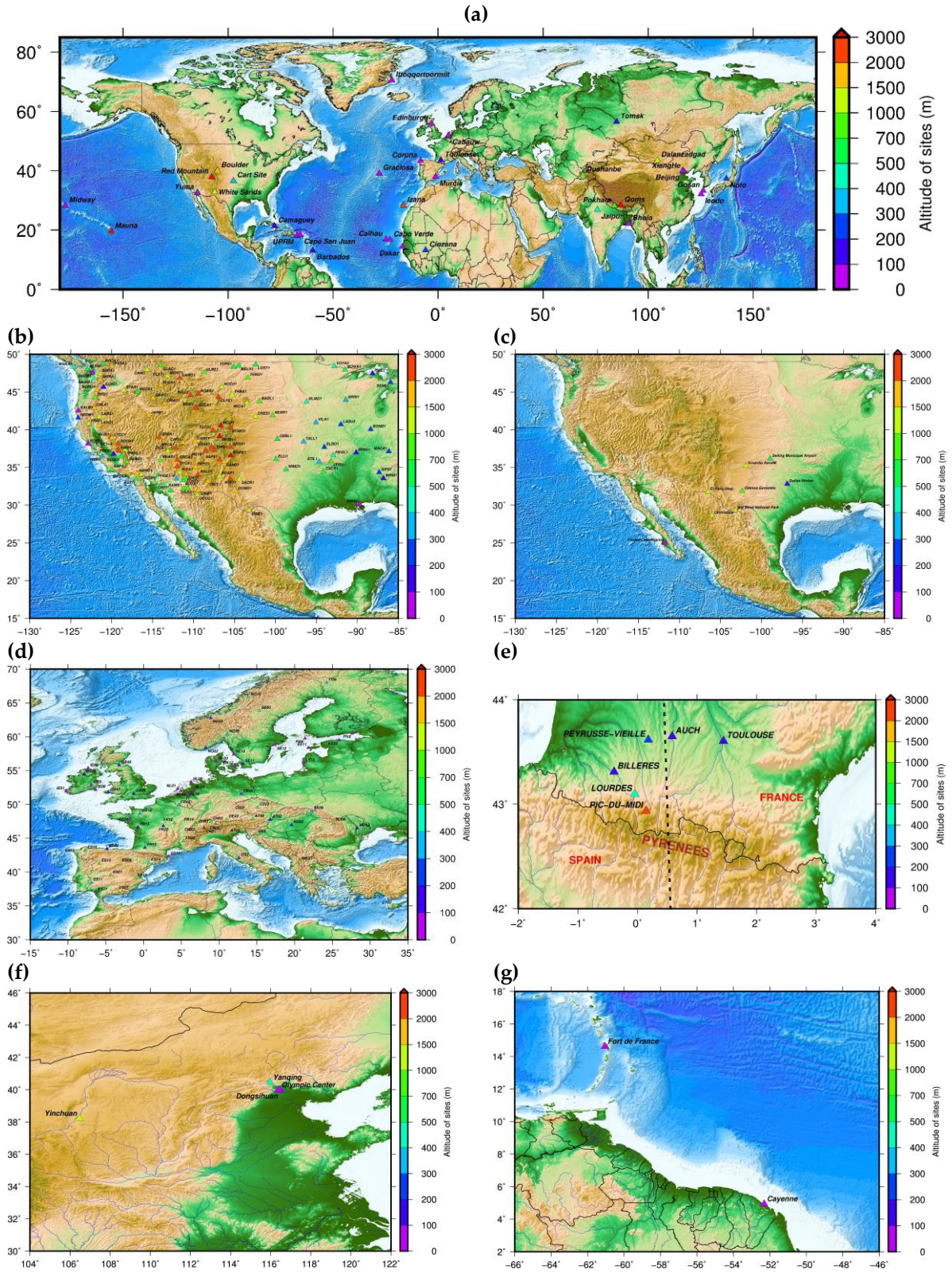

Figure S6. Map of site locations presented in the publication for AERONET stations (a), IMPROVE stations (b), US EPA networks for PM2.5 data (c), EBAS-EMEP stations (d) see Table S2 for the names of EMEP stations, French stations close to the Pyrenees area (e), Chinese stations (f) and the two stations in the Caribbean area (g).

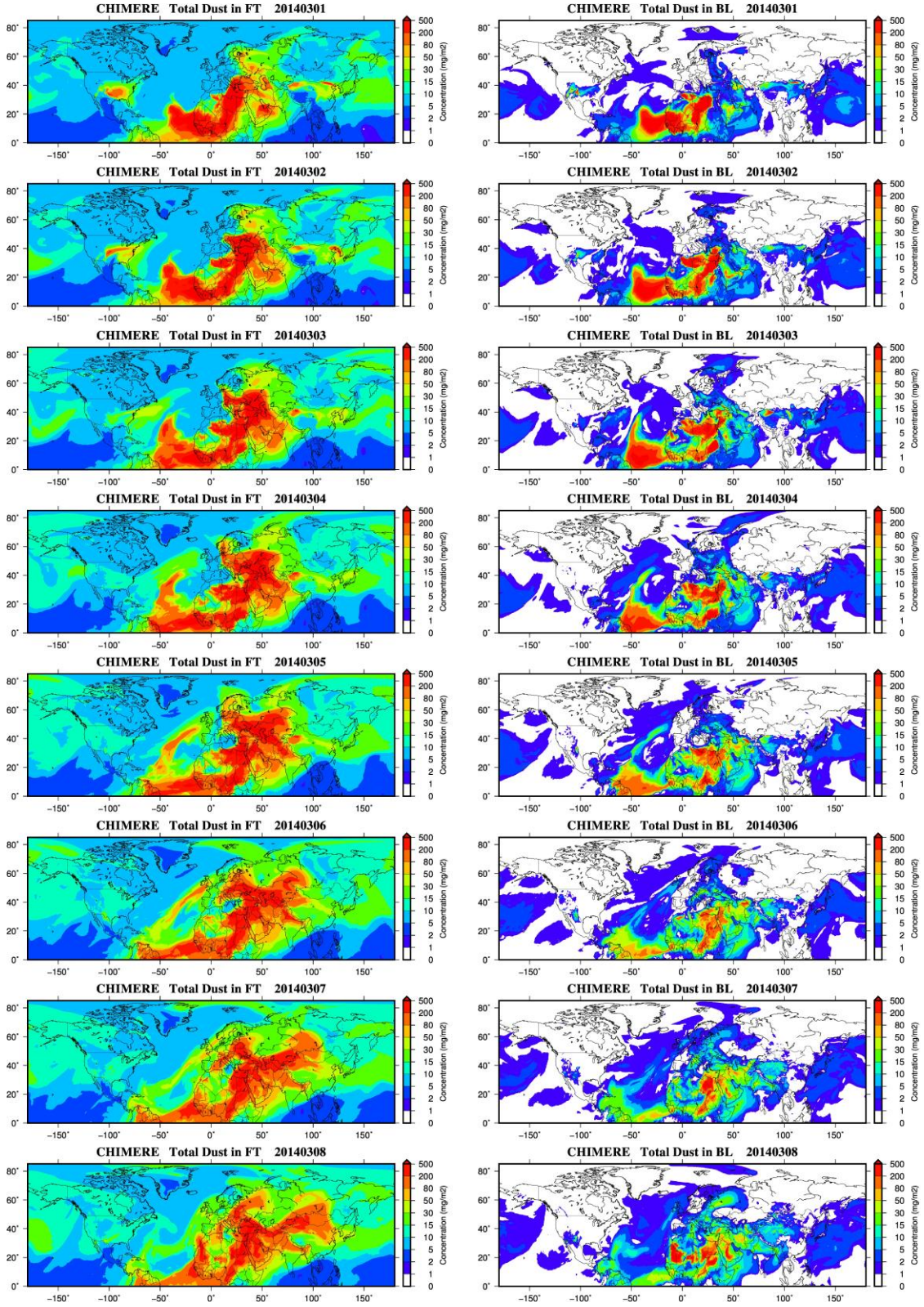

Figure S7. Evolution of mean daily concentrations integrated over the column (in g m^{-2}) of total dust from March 1st, to March 8th, 2014 in the free troposphere (FT) and the boundary layer (BL)

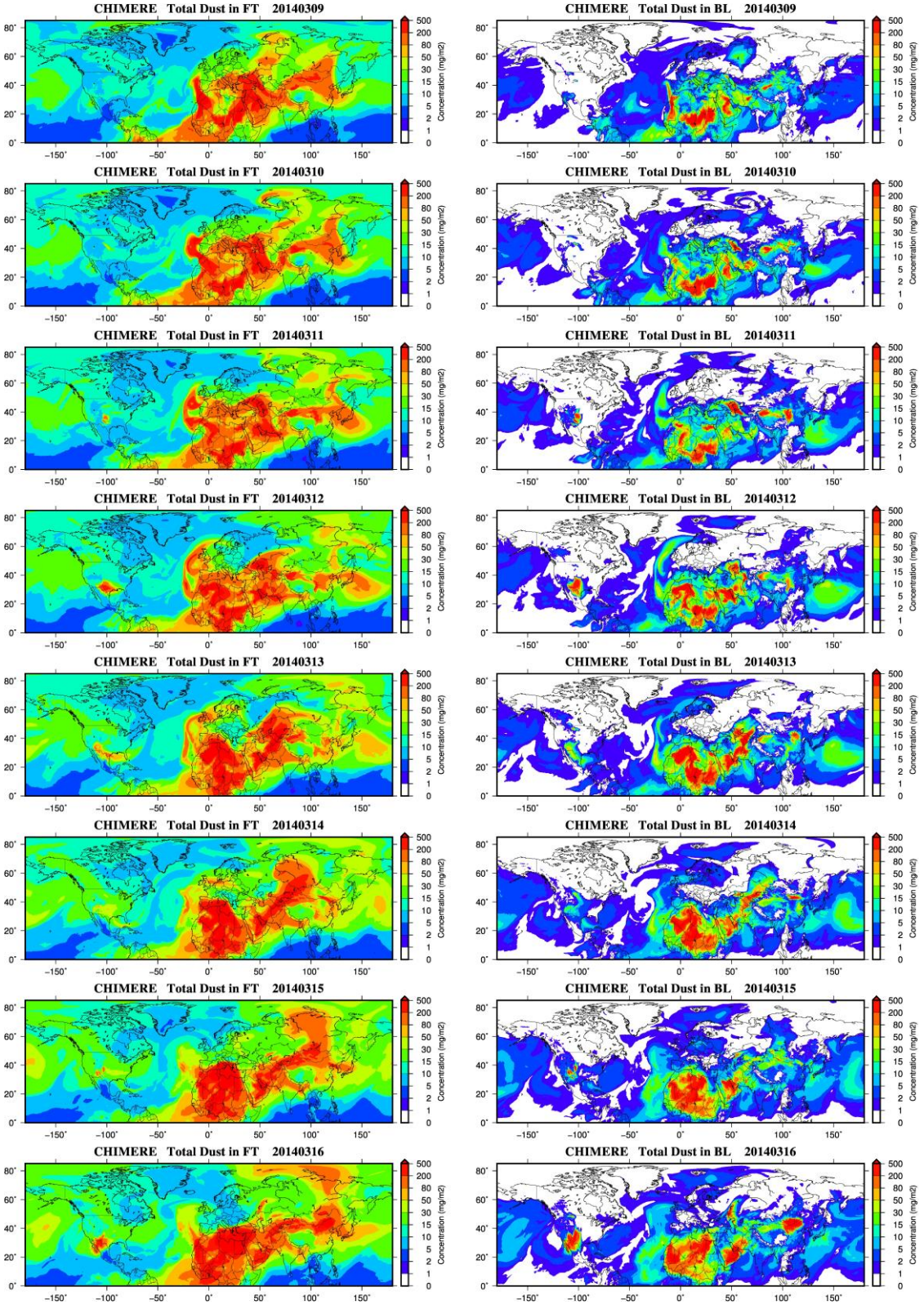

Figure S8. Evolution of mean daily concentrations integrated over the column (in g m^{-2}) of total dust from March 9th, to March 16th, 2014 in the free troposphere (FT) and the boundary layer (BL)

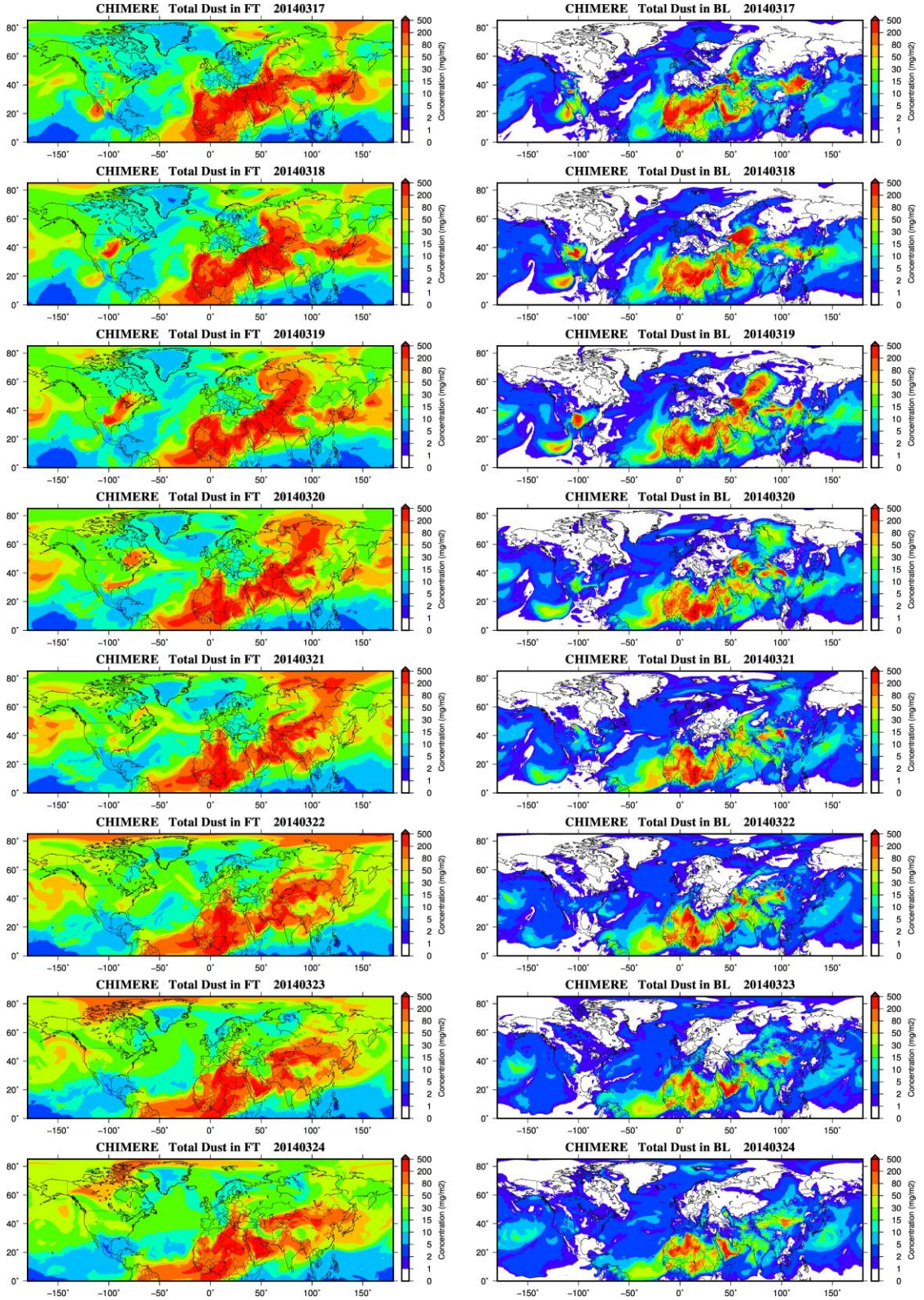

Figure S9. Evolution of mean daily concentrations integrated over the column (in g m^{-2}) of total dust from March 17th, to March 24th, 2014 in the free troposphere (FT) and the boundary layer (BL)

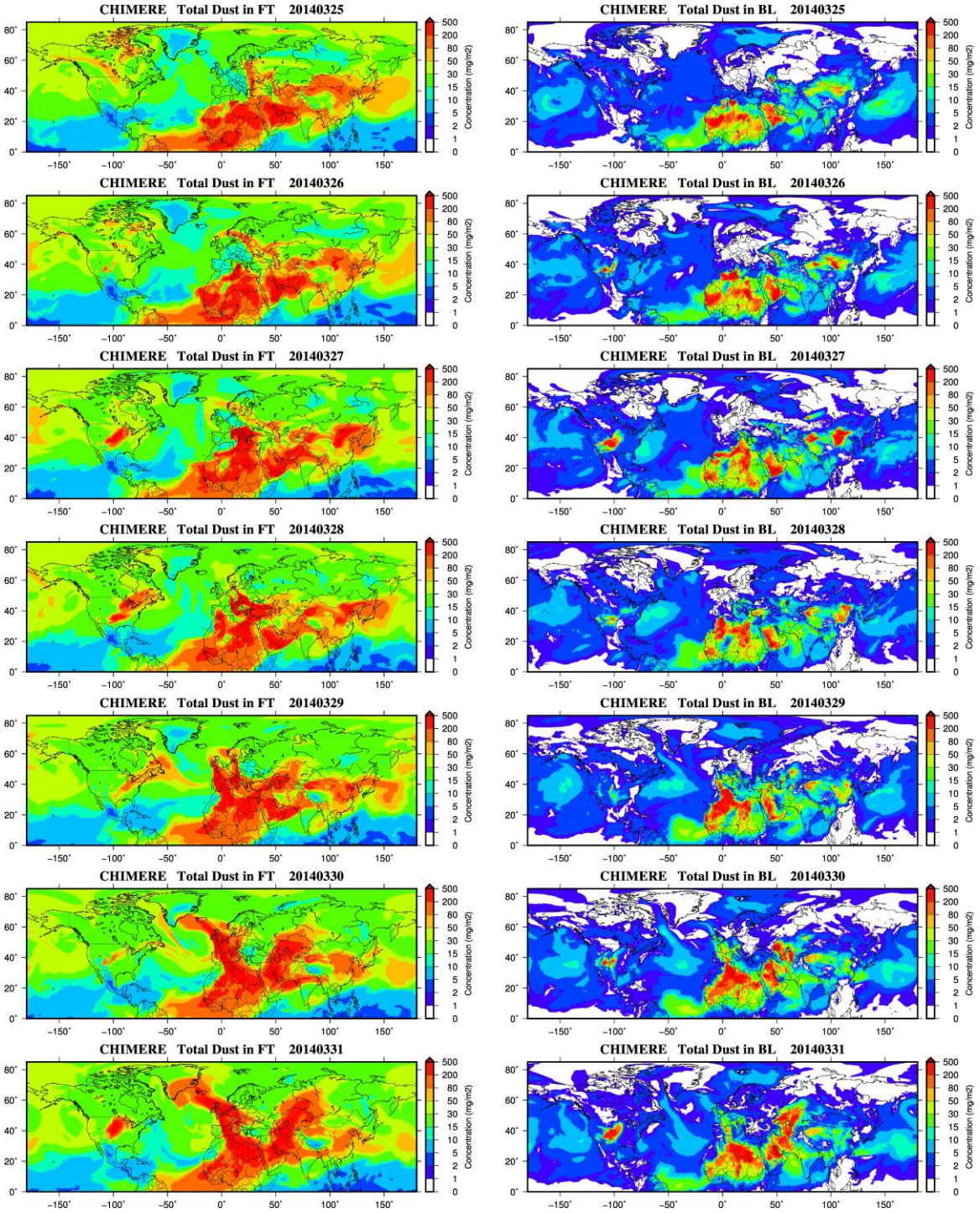

Figure S10. Evolution of mean daily concentrations integrated over the column (in g m^{-2}) of total dust from March 25th, to March 31st, 2014 in the free troposphere (FT) and the boundary layer (BL)

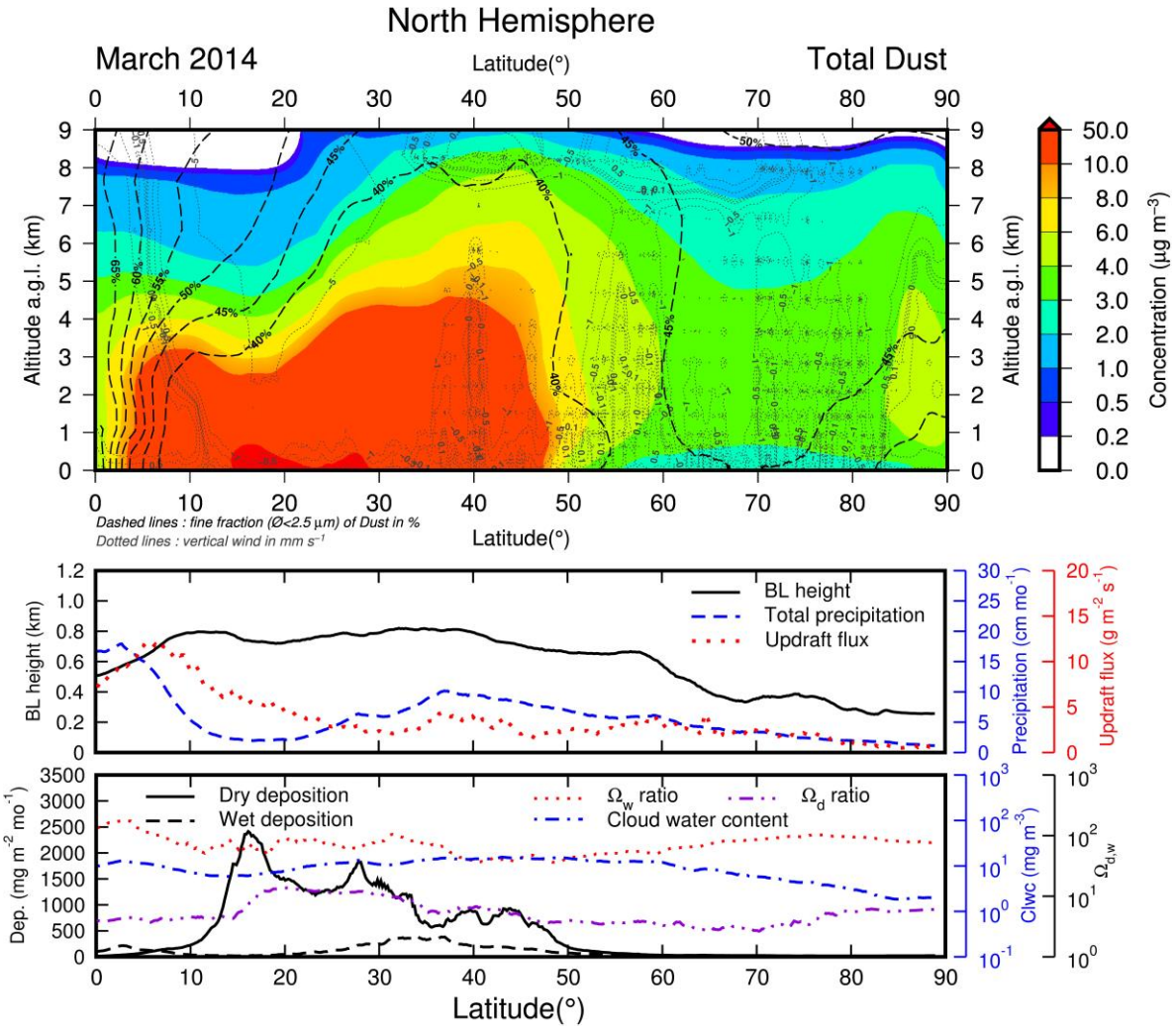

Figure S11. Monthly mean latitudinal cross sections (Altitude a. g. l. *versus* Latitude °N) for several variables in March 2014 simulated by CHIMERE over the north hemisphere. <u>Top panels</u> represent the mean dust concentrations with bold dashed lines representing the fine fraction of total dusts (%), the grey dotted lines are the average zonal winds (conventionally, westerly wind are positive). <u>Bottom charts</u> represent the evolution of various parameters along the corresponding cross sections and spatially averaged over the longitude: the boundary layer (BL) height in km, the total precipitation (convective and large scale) in cm month^{-1}, the deep convection updraft flux summed over the column in g_{air} m^{-2} s^{-1}, the mean cloud water content averaged over the first 10 model layers (approximatively 2500m), the wet and dry deposition fluxes of dust sum over time (monthly) in mg_{dust} m^{-2} month^{-1} and the ratio Ω (unit less) of dry (d) and wet (w) scavenging coefficients coarse *versus* fine particles as defined in equation 2 in the publication).

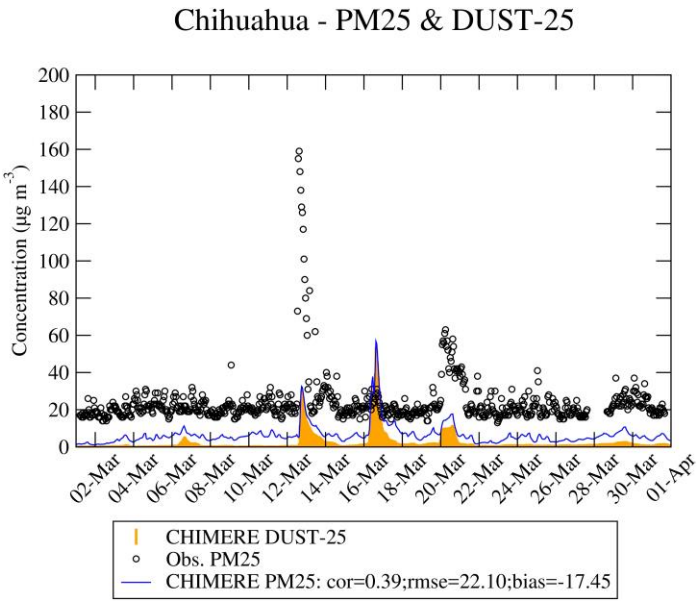

Figure S12. PM2.5 time series at Chihuahua station (Mexico) for CHIMERE and the corresponding observations. The orange shade area represents the dust in the PM2.5 matrix simulated by CHIMERE.

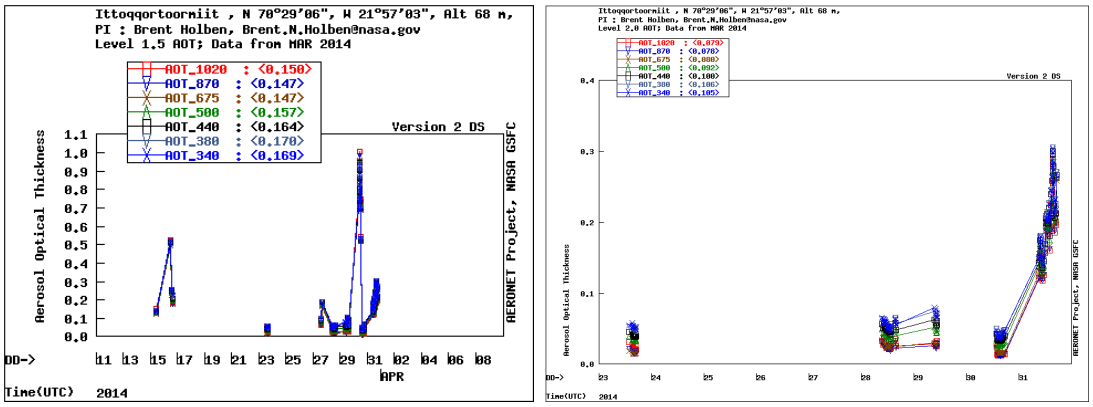

Figure S13. AOD from AERONET network at Ittoqqortoomitt in March 2014, level 1.5 (left) and level 2 (right) (source: NASA, https://aeronet.gsfc.nasa.gov/)

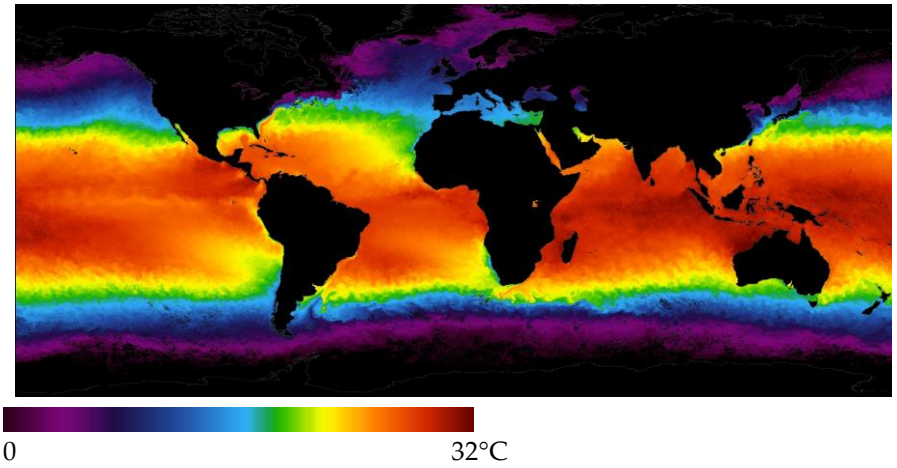

Figure S14. Mean sea surface temperature in March 2014 (source: NASA https://worldview.earthdata.nasa.gov)

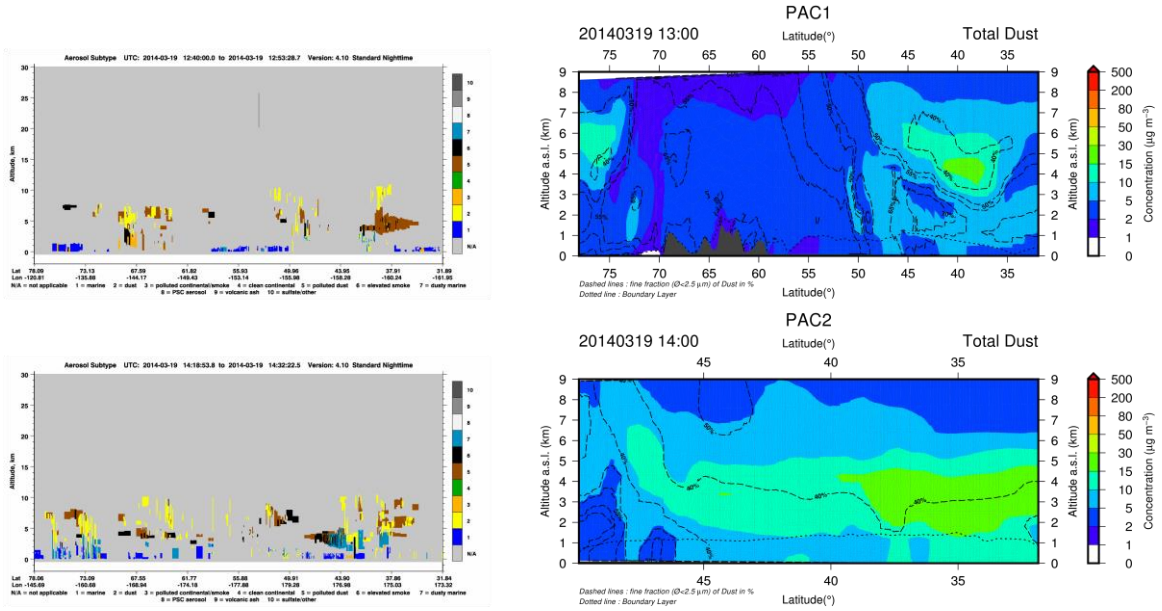

Figure S15. Cross sections of CHIMERE dust concentrations (right) for several orbits zoomed over the highest values area *versus* the corresponding CALIPSO qualitative data (left) showing in yellow the dust load and in orange the polluted dust, for the CALIPSO trajectories PAC-1-2 as reported in Figure 2 in the publication. The dotted line represents the height of the boundary layer, the dashed lines represent the fraction of fine dust in %.

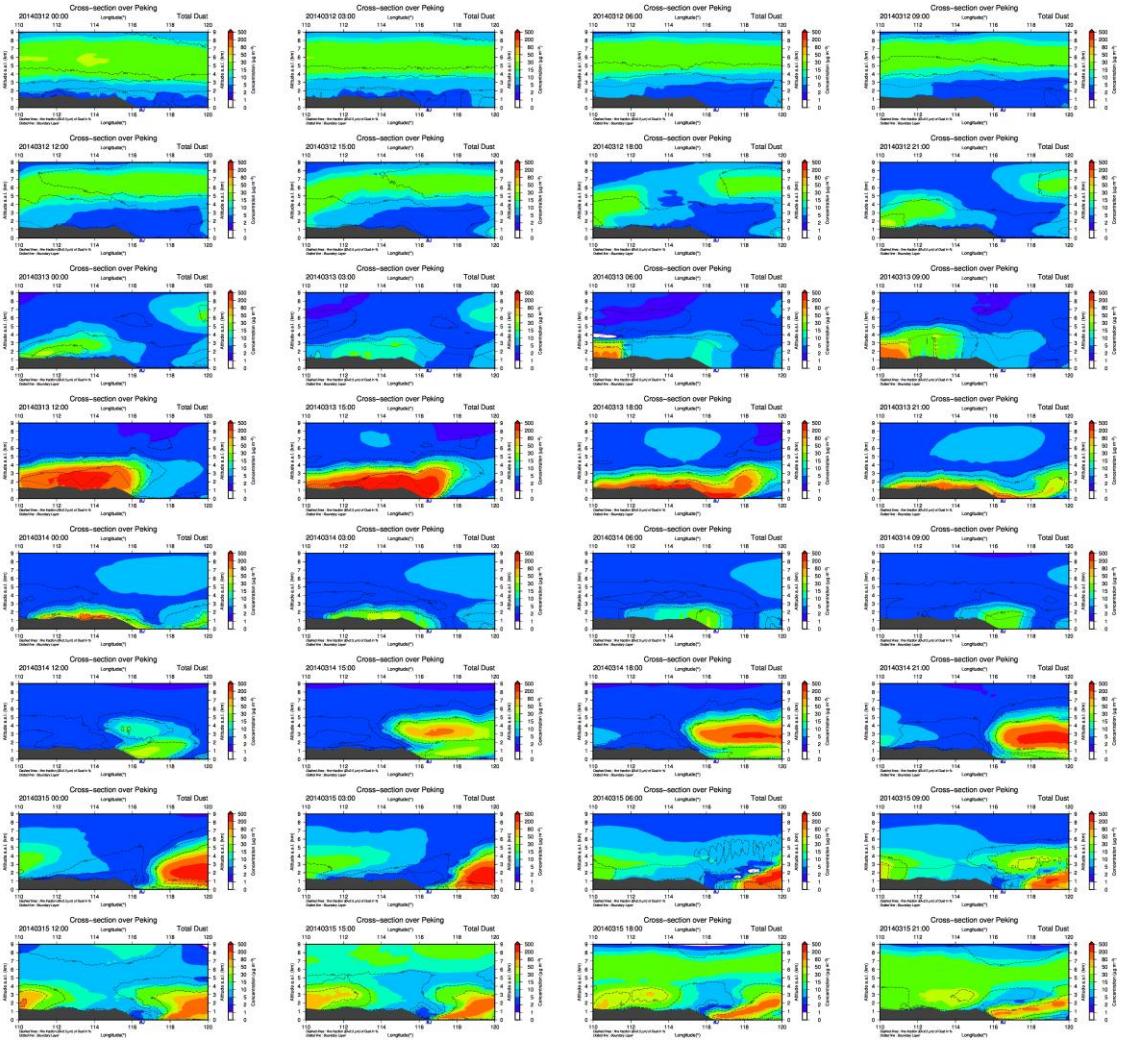

Figure S16. Longitudinal cross section of total dust concentrations fields (Altitude *versus* longitude) at 39.9°N latitude from 110°E to 120°E passing over Beijing (BJ in blue letters) from March 12th 00:00 UTC to March 15th, 21:00 UTC. The dotted line represents the height of the boundary layer, the dashed lines represent the fraction of fine dust in %.

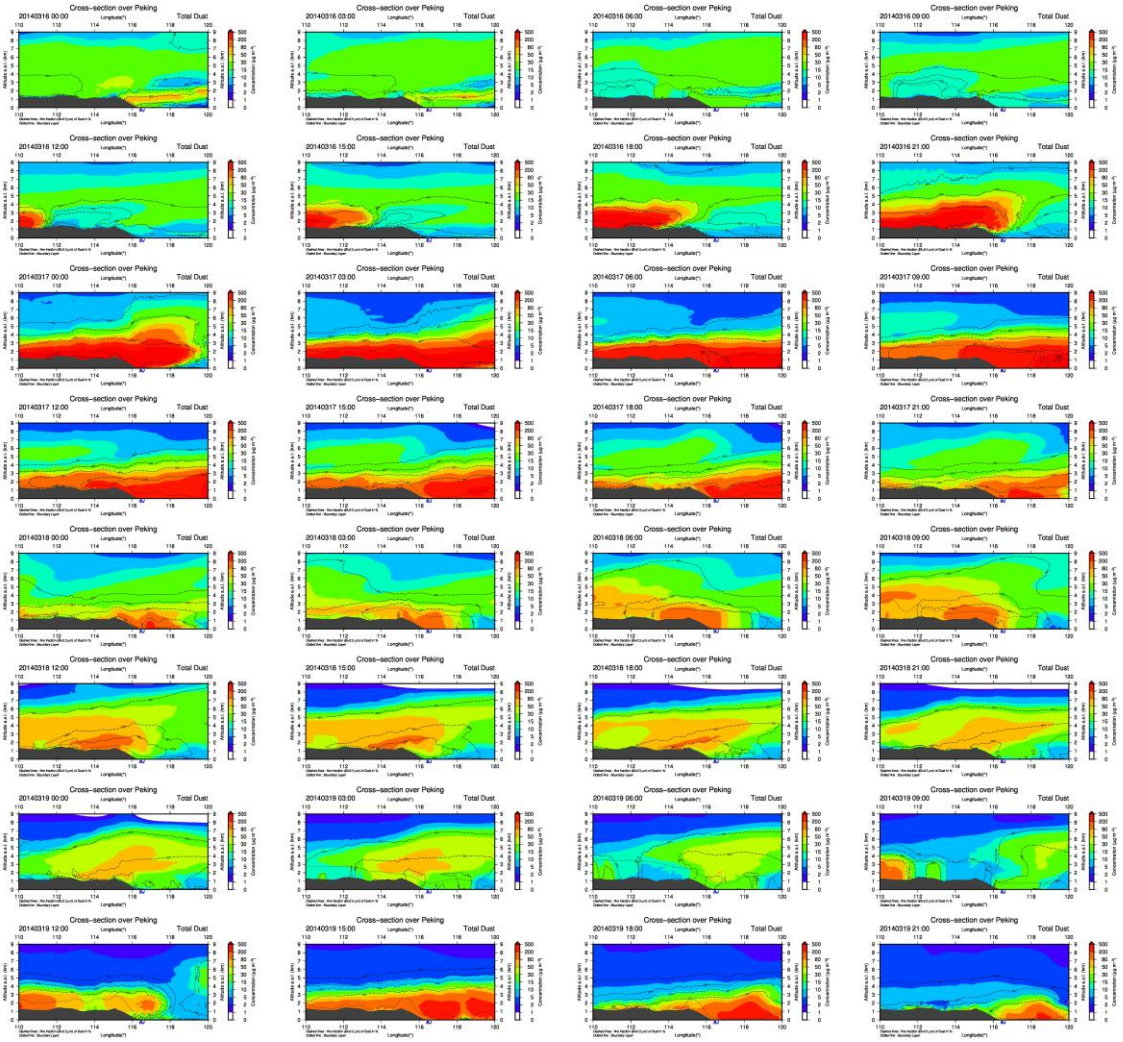

Figure S17. Longitudinal cross section of total dust concentrations fields (Altitude *versus* longitude) at 39.9°N latitude from 110°E to 120°E passing over Beijing (BJ in blue letters) from March 16th 00:00 UTC to March 19th, 21:00 UTC. The dotted line represents the height of the boundary layer, the dashed lines represent the fraction of fine dust in %.